ACS APPLIED MATERIALS & INTERFACES

Research Article

www.acsami.org

Enhanced Cycling Stability of Lithium Sulfur Batteries Using Sulfur–Polyaniline–Graphene Nanoribbon Composite Cathodes

Lei Li,[†] Gedeng Ruan,[†] Zhiwei Peng,[†] Yang Yang,[†,‡] Huilong Fei,[†] Abdul-Rahman O. Raji,[†] Errol L. G. Samuel,[†] and James M. Tour*[,†,‡,§]

[†]Department of Chemistry, [‡]Richard E. Smalley Institute for Nanoscale Science and Technology, and [§]Department of Materials Science and NanoEngineering, Rice University, 6100 Main Street, Houston, Texas 77005, United States

Supporting Information

ABSTRACT: A hierarchical nanocomposite material of graphene nanoribbons combined with polyaniline and sulfur using an inexpensive, simple method has been developed. The resulting composite, characterized by scanning electron microscopy, transmission electron microscopy, X-ray photoelectron microscopy, and X-ray diffraction analysis, has a good rate performance and excellent cycling stability. The synergistic combination of electrically conductive graphene nanoribbons, polyaniline, and sulfur produces a composite with high performance. The method developed here is practical for the large-scale development of cathode materials for lithium sulfur batteries.

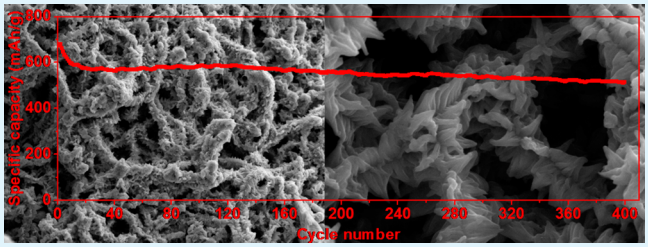

KEYWORDS: *lithium sulfur battery, polyaniline, graphene nanoribbons, sulfur, energy storage*

1. INTRODUCTION

The development of high capacity energy storage systems is important for portable electronic devices, power tools, and electric vehicles.[1−4] Lithium sulfur batteries (LSBs) have attracted attention as potential energy storage devices because the sulfur cathode in LSBs has a high theoretical capacity of 1672 mA·h/g and an energy density of 2567 W·h/kg, almost 5 times higher than conventional cathodes, presuming complete reaction of lithium with sulfur to form Li_2S.[5−8] Elemental sulfur is inexpensive, nontoxic, and abundant in nature.[8,9] However, the practical applications of LSBs are limited by two challenges. The first challenge is that sulfur is electrically insulating.[10,11] The second is the severe degradation of the lithium sulfur battery cycle life, a result of the volume change and high solubility of the polysulfide products.[5,12,13] When sulfur is fully converted to Li_2S, the volume increases as much as 80%, which leads to the fading capacity because of the pulverization of battery materials. The high solubility of polysulfide products makes it more likely that they will take part in the sulfur shuttle mechanism, resulting in capacity decay due to the loss of sulfur active materials through redox reactions of lithium polysulfide at both the cathode and anode surfaces.

Extensive effort has been devoted to address these challenges of sulfur's insulating nature and the capacity decay. The poor electrical conductivity of sulfur can be improved by the introduction of conducting materials that form composites, such as graphene,[14,15] carbon nanotubes,[16] conducting polymers,[13,17,18] and other carbon matrixes.[19−22] Many strategies have been developed to enhance the cycling life of LSBs. For example, the electrolyte additive $LiNO_3$ has been shown to be effective in reducing the capacity decay because it enhances the stability of polysulfide in the electrolyte, protects the lithium anode from electrochemical and chemical reactions, and reduces the viscosity of the liquid electrolyte.[23−25] Another method is to protect the anode in LSBs, which can reduce the sulfur shuttle effect, improving the cycling performance.[23,26,27] Various matrixes have been developed to trap the soluble intermediate lithium polysulfide, such as mesoporous carbon,[22] amorphous carbon,[28] carbon nanotubes,[16,29] graphene,[14,15] hollow carbon spheres,[30,31] metal oxides,[32,33] and conducting polymers.[13,17,34] Among all these matrixes, conducting polymers open new possibilities for the cycling life improvement in the LSBs due to their easy preparation and scale-up, mechanical structure, self-healing, and good electrical conductivity.[12,35] For example, Wu et al. prepared the composite sulfur/polythiophene with a core−shell structure, which showed good cycling stability of 67.5% capacity retention after 80 cycles.[17] Xiao et al. synthesized a composite sulfur−polyaniline that improved the cycling life of LSBs with only 24% capacity decay after 500 cycles.[13] Polyaniline is an interesting conducting polymer because it works as a substrate to load sulfur and can be used as a cathode in lithium sulfur batteries. However, polyaniline suffers from two major problems which hinder its application in lithium sulfur batteries. The first problem is the limited electrical conductivity, and the other is the mechanical degradation caused by its large volumetric change, leading to its poor cycling stability in energy storage devices. Therefore, to mitigate these negative effects, it

Received: May 15, 2014
Accepted: August 20, 2014
Published: August 20, 2014

 © 2014 American Chemical Society

is important to improve polyaniline related materials for lithium sulfur batteries.

In this study, a unique structure where sulfur was loaded on polyaniline−graphene nanoribbons (PANI−GNRs) was designed to reduce the capacity decay in lithium sulfur batteries. The PANI−GNR composite was prepared by the in situ polymerization of aniline in the presence of GNRs.[36,37] GNRs serve as the substrate for polyaniline growth, and increase the electronic conductivity and effective utilization of PANI in the composite. The GNRs also improved the mechanical properties of the composite, resulting in an enhancement of its ability to recover from the volume expansion.[36] Therefore, PANI−GNRs effectively overcome the negative deficiencies of PANI alone.

Sulfur−PANI−GNRs (SPGs) were prepared by heat treatment of a mixture of elemental sulfur and PANI−GNRs.[13] In the SPGs, PANI−GNRs work as an electronic conductivity framework for sulfur and they enhance the mechanical properties of SPGs. A fraction of the sulfur reacts with polyaniline to form a cross-linked network with the interchain or intrachain disulfide bond interconnectivity during the vulcanization process.[13] The rest of the sulfur diffuses into the hierarchical network of PANI−GNRs and newly formed polymer networks. PANI traps the soluble intermediate lithium polysulfide through strong physical and chemical absorption effects.[13] The GNR reinforcement reduces the damage that normally occurs from volume change during the electrochemical reaction. Therefore, SPGs as cathode materials demonstrate excellent cycling performance due to the synergetic effect of GNRs, PANI, and sulfur.The stable reversible specific discharge capacity is 567 mA·h/g at the 26th cycle, and it only decays 9% in the following 374 cycles, at the rate of 0.4 C. Therefore, SPGs are outstanding candidates for use as cathode materials for energy storage in LSBs.

2. EXPERIMENTAL SECTION

2.1. Synthesis of PANI−GNRs and Polyaniline (PANI). GNRs,[37] PANI, and PANI−GNRs were prepared as described previously.[36] GNRs were prepared by treatment of multiwalled carbon nanotubes with NaK in 1,2-dimethoxyethane and quenching of the reaction with MeOH. In order to increase their wettability, GNRs (100 mg) were refluxed in 3 M HNO_3 (400 mL) for 12 h. HNO_3-treated GNRs (22.5 mg) were added to 1 M H_2SO_4 (40 mL), and the dispersed GNR solution was formed by sonication (2510 Branson) for 2 h. Aniline (900 mg, 9.65 mmol) was added to the above dispersion and with stirring to form a uniform mixture in a NaCl−ice bath (−3 to −5 °C). The oxidant ammonium persulfate (APS) (554 mg, 2.4 mmol) was dissolved in 40 mL of 1 M H_2SO_4 and cooled in the NaCl−ice bath for 10 min. Then, the two solutions were mixed with continuous stirring in the NaCl−ice bath for 10 h. The black solid sample was collected by vacuum filtration with sequential washing with water and acetone. The final PANI−GNRs (130 mg) were obtained after drying in a vacuum oven (∼10 mmHg) at 85 °C for 10 h. PANI was prepared using the same method above without the addition of GNRs.

2.2. Synthesis of Sulfur−PANI−GNRs (SPGs) and Sulfur−Polyaniline (SP). Sulfur (200 mg) was dissolved in carbon disulfide (1 mL). PANI−GNRs (50 mg) were added to the solution with continued magnetic stirring for 30 min at room temperature in order to achieve a good dispersion. Then, the mixture was stirred in an open reaction flask in the hood until the carbon disulfide evaporated. The resulting solid mixture was sealed in a vessel under N_2. The heat treatment of the mixture proceeded in two steps. The mixture was first heated at 155 °C for 12 h, and then the temperature was raised to 280 °C for another 12 h to complete the vulcanization reaction. SPGs (100 mg) were obtained after the mixture was permitted to cool to room temperature. Unreacted sulfur remained on the walls of the flask. For comparison purpose, SP was obtained using a similar procedure between polyaniline and sulfur.

2.3. Materials Characterization. Products were characterized by X-ray diffraction (XRD; Rigaku D/Max Ultima II), X-ray photoelectron spectroscopy (XPS; PHI Quantera), scanning electron microscopy (SEM; JEOL 6500), thermogravimetric analysis (TGA; TA Instruments, Q50), and transmission electron microscopy (TEM; JEM2100F TEM).

2.4. Electrochemical Measurements. To form a slurry, 80 wt % active materials (SPGs, SPs, and S), 10 wt % carbon black (Super P, TIMCAL), and 10 wt % polyvinylidene difluoride (PVDF; Alfa Aesar) were dissolved in *N*-methyl-2-pyrrolidone (NMP; Sigma-Aldrich). Then, the slurry was coated on an aluminum foil substrate to form the cathodes. The typical mass loading of the active materials is around 1.2 mg/cm^2. Electrochemical tests were performed using CR2032 coin-type cells with lithium metal foil as the counter electrode. The electrolyte was 1 M lithium bis(trifluoromethane) sulfonimide (LiTFSI) dissolved in a mixture of 1,3-dioxolane (DOL) and dimethyoxyethane (DME) (1:1 v:v) with 1 wt % $LiNO_3$, and the separator was a Celgard 2300 membrane. Cyclic voltammetric (CV) tests were done on a CHI660D electrochemical station at a current density of 0.60 mV/s. The galvanostatic discharge charge test was carried out on a LAND CT2001A battery system at room temperature. The capacity was evaluated based on the mass of the sulfur in the composite.

3. RESULTS AND DISCUSSION

3.1. Synthesis and Structure Analysis. The synthesis of the SPGs, as described in the Experimental Section, is schematically depicted in Scheme 1.[13]

Scheme 1. Schematic Illustration of the Synthesis of SPGs

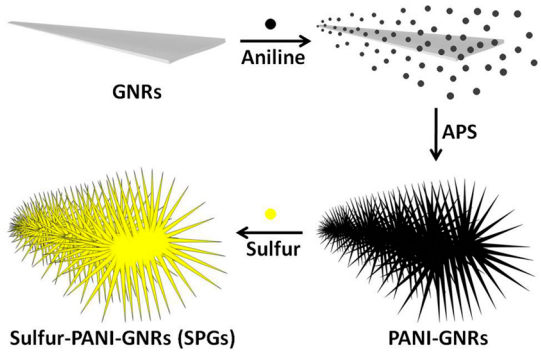

The morphologies of SPGs, SP, PANI−GNRs, and PANI were characterized by SEM and TEM as shown in Figure 1 and Figure S1 (Supporting Information). Parts a and b of Figure 1 are the low and high resolution SEM images of SPGs, respectively. The ordered, vertically aligned PANI was directly growing on and around the GNRs with a brushlike structure. The morphology was well maintained after the sulfur loading compared to PANI−GNRs as shown in Figure S1a (Supporting Information). The structure was also established by the TEM images as shown in Figure 1c,d. The structure of SPGs was further studied by the elemental mapping of carbon, nitrogen, oxygen, and sulfur. As shown in Figure 1e−h, these elements were uniformly distributed in the SPGs. TEM images of SPGs revealed that sulfur was homogeneously loaded on PANI nanorods and the morphology of PANI−GNRs was still well maintained. As shown in Figure S1b (Supporting Information), irregular PANI was intertwined together. PANI could not form the brushlike structure without the graphene nanoribbons. After the sulfur loading, the morphologies of SPs had no

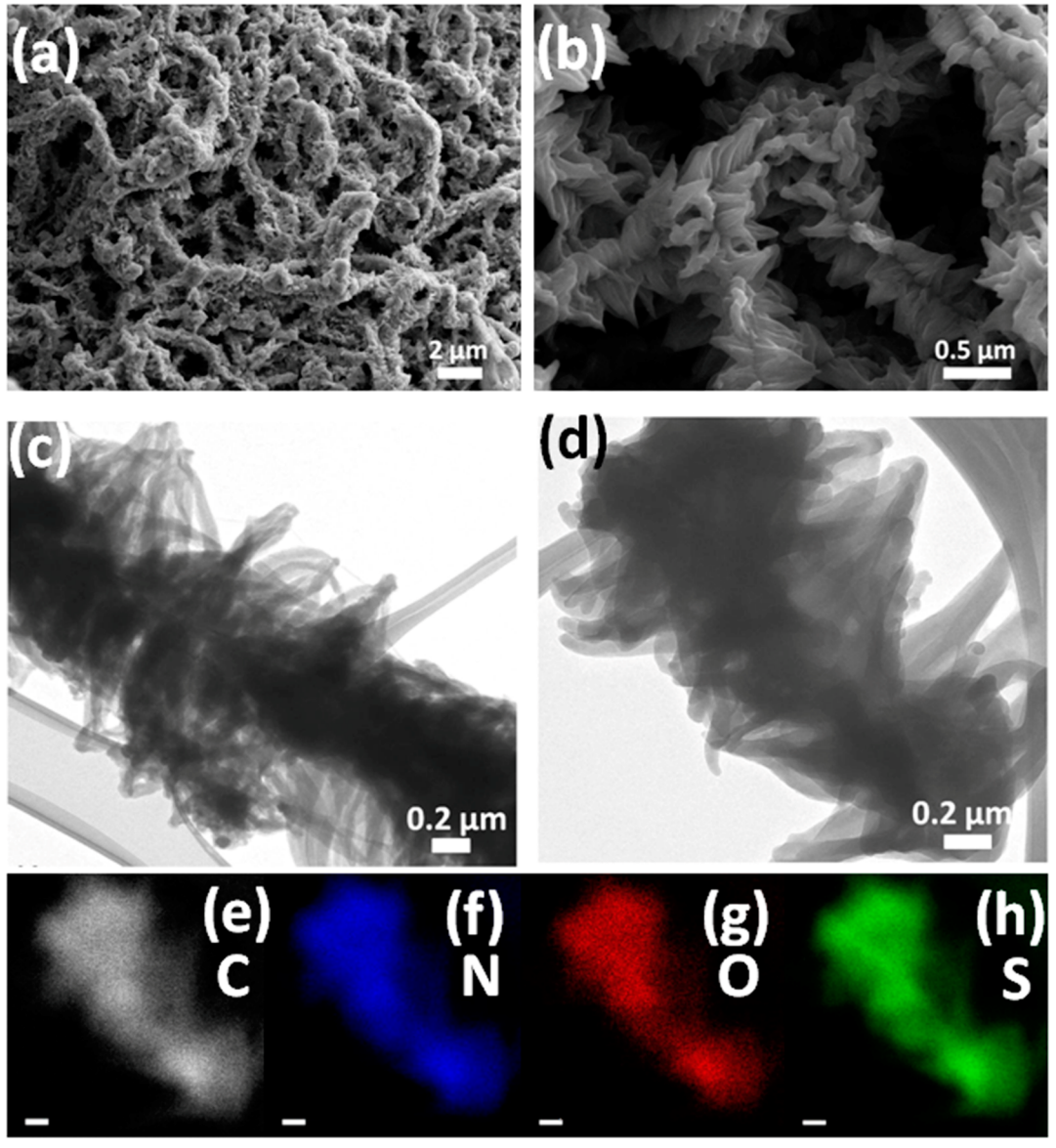

Figure 1. (a, b) SEM images of SPGs at different resolutions. (c, d) TEM images of SPGs and corresponding elemental mapping of (e) carbon, (f) nitrogen, (g) oxygen, and (h) sulfur. The scale bars in (e)−(h) are 0.2 μm.

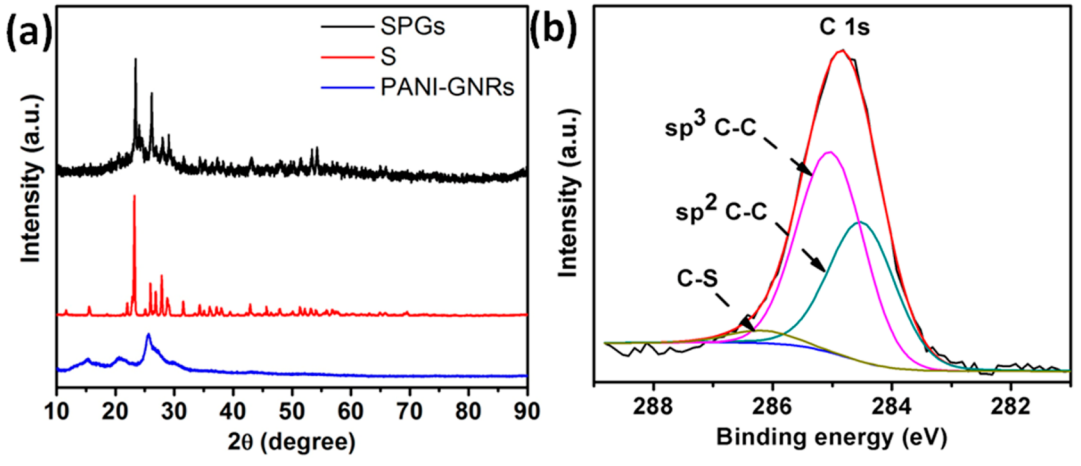

Figure 2. (a) XRD patterns of sulfur, PANI−GNRs, and SPGs. (b) C 1s core level XPS of SPGs.

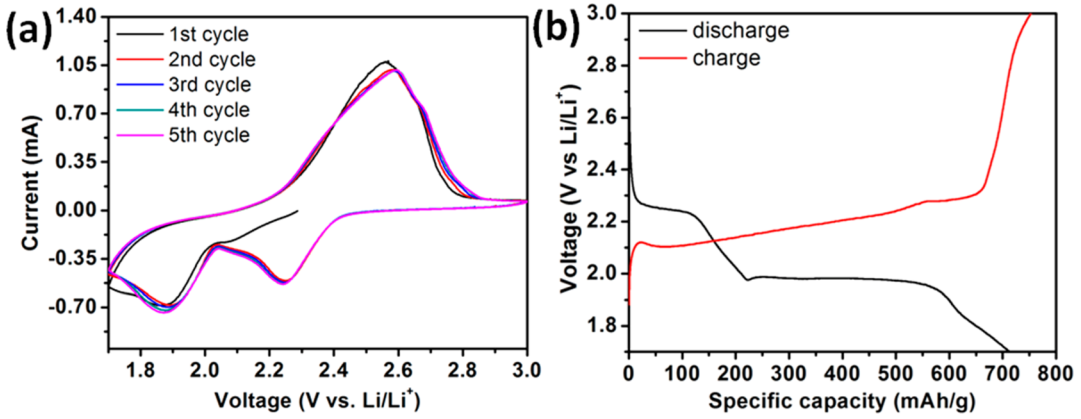

Figure 3. (a) First five cyclic voltammograms of composite SPGs at a sweep rate of 0.4 mV s^{-1}. (b) Discharge and charge voltage vs specific capacity profiles at 3.0−1.7 V at 0.1 C.

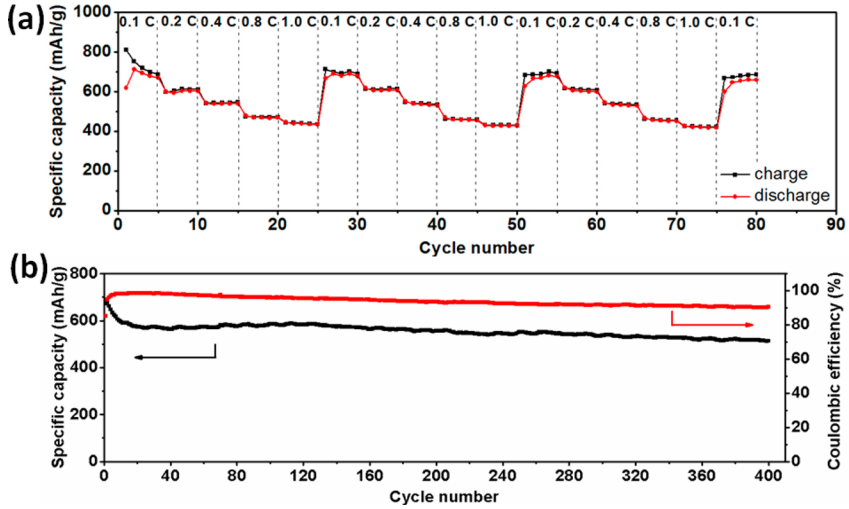

Figure 4. (a) Rate performance of SPGs at various rates from 0.1 to 1.0 C with respect to cycle numbers. (b) Cycling performance of SPGs at a rate of 0.4 C.

obvious change as shown in Figure S1c−f (Supporting Information).

XRD and XPS were also used to characterize the SPGs and SPs. Figure 2a shows the XRD pattern of PANI−GNRs, sulfur, and composite SPGs. The XRD pattern of PANI−GNRs showed the four characteristic peaks at 2θ of 15.3, 21.0, 25.6, and 26.5°.[37−39] The XRD pattern of composite SPGs had peaks similar to those of sulfur, including the obvious increase in peak intensity of 2θ at 26.1° due to the incorporation of sulfur into PANI−GNRs and a new peak at 21.0° because of the PANI−GNRs in the composite. XPS indicates that the composite SPGs only contained four elements, S, C, N, and trace O, from the APS and/or sulfuric acid (Supporting Information, Figure S2). As shown in Figure 2b, the deconvolution of the C 1s core level XPS of SPGs leads to three peaks, resulting from three different electronic states. The peaks with binding energy of 284.5 eV can be attributed to sp^2 hybridized carbon atoms, those with binding energy of 285.0 eV can be attributed to sp^3 hybridized carbon atoms, and those with binding energy of 286.2 eV can be attributed to carbon−sulfur chains.[40] For comparison, SPs were also characterized by XPS and XRD, which proved sulfur was successfully loaded on PANI as shown in Figure S3 (Supporting Information). TGA analysis of SPGs showed 62% sulfur content in the composite as shown in Figure S4a (Supporting Information), while 59% sulfur content was obtained in SPs (Figure S4b, Supporting Information).

3.2. Electrochemical Evaluation. In order to evaluate the electrochemical performance of SPGs as cathodes in LSBs, cyclic voltammetry (CV) and galvanostatic discharge charge experiments were carried out in CR2032 coin cells. Figure 3a shows the CV that was used to study the electrochemical reaction mechanism of the SPG cathodes in the LSBs in the potential range 1.7−3.0 V.[23] During the cathodic reduction process, there are two peaks at 2.25 and 1.88 V (vs Li/Li^+). According to the reaction mechanism of sulfur reduction and oxidation during the discharge and charge processes,[1,23,41] the peak at 2.25 V results from the reduction of sulfur to higher-order polysulfides. The peaks at 1.88 V correspond to the reduction of sulfur from higher-order polysulfides to Li_2S_2/Li_2S. In the subsequent anodic scan, a broad oxidation peak was observed at 2.56 V with a shoulder at 2.67 V in the first cycle; the peak shifted to 2.60 V with a shoulder peak at 2.67 in the following cycles. The two overlapping oxidation peaks related to the conversion among Li_2S, polysulfides, and elemental sulfur. After the first cycle, both the peak positions and area of the CV peaks remain almost without obvious change, demonstrating relatively good capacity retention. For comparison, Figure S5 in the Supporting Information shows the CV

profile of SPs and sulfur with little difference between the two. Figure 3b shows the voltage profile of SPGs at the rate of 0.1 C. There were two obvious plateaus in the discharge curve, relating to the formation of higher-order polysulfides and Li_2S_2/Li_2S. This result was consistent with the CV. The stable, reversible discharge capacity of the second cycle can reach 714 mA·h/g.

The rate performance of the SPGs was studied in the same potential range as shown in Figure 4a. For the first five cycles, the capacity decreased with the increase in cycle numbers at the rate of 0.1 C. A stable capacity at different current densities was observed. When the rate was reduced from 1.0 to 0.1 C, the value of the specific capacity of SPGs was still 688 mA·h/g at the 80th cycle. The rate performance demonstrates that the SPGs remained stable after extended rate cycles. The cycling performance for SPGs was also evaluated by discharge−charge experiments. For comparison, SPs and sulfur were first tested as cathodes in the LSBs at the rate of 0.4 C. The specific capacity of SPs can reach 614 mA·h/g at the ninth cycle as shown in Figure S6a (Supporting Information). However, it deceased quickly in the following cycles with only 417 mA·h/g at the 90th cycle. For the pure sulfur cathode, the specific discharge capacity quickly decreased to 120 mA·h/g at the 100th cycle from 291 mA·h/g at the second cycle; only 41% capacity remained as shown in Figure S6b (Supporting Information). This demonstrated that PANI increased the specific capacity and cycling stability of sulfur cathodes. Figure 4b shows the cycling performance of SPGs tested under the same conditions. The specific discharge capacity was 673 mA·h/g in the first cycle and decreased to 567 mA·h/g in the 26th cycle due to the loss of sulfur at the surface of SPGs. Then, the specific discharge capacity increased slightly with the increase in cycle numbers, and reached 588 mA·h/g at the 113th cycle. In the following cycles, the value of the specific discharge capacity decreased slowly as the cycle numbers increased and reached 514 mA·h/g at the 400th cycle. A capacity decay of 9% occurred after 374 cycles from the 26th cycle. The Coulombic efficiency of SPGs quickly increased to almost 100% in several cycles and stayed optimal for more than 30 cycles. Then, it decreased with the increase in cycles but was maintained over 90% when the cycles increased to 400. It is presumed that the PANI−GNRs could not completely trap the polysulfide, and the additive $LiNO_3$ was consumed during the discharge and charge process.[24] The shuttle effect was still present, leading to a lower Coulombic efficiency when the batteries operated for extended periods. The graphene nanoribbons indeed enhanced mechanical properties of PANI−GNRs, which improved the cycling stability of SPGs during the extended cycles. Therefore, PANI−GNRs effectively trapped the polysulfide during the discharge and charge processes, resulting in great improvements in the cycling performance of the LSBs.

In order to study the electrochemical performance of the SPGs in LSBs, electrochemical impedance spectroscopy (EIS) experiments were carried out after five cycles for sulfur, SPs, and SPGs as shown in Figure 5a. Figure 5b shows the equivalent circuit model of this system.[17,42] In this model, R_s is the internal resistance of the tested battery, R_p and R_{ct} represent the passivation film and charge-transfer resistance, respectively, CPE_1 and CPE_2 are associated with the constant phase element of space charge capacitance and double layer capacitance, respectively, and Z_w is the Warburg resistance related to the lithium diffusion process. In Figure 5a, the plots consist of two semicircles in the high and intermediate frequency ranges and a sloping line with an angle of ~45° to the real axis in the low frequency region. The two semicircles result from the Li^+ ion transport through the passivation film and the interfacial charge transfer reaction (R_p and R_{ct}) combined with the electrochemical capacitive behaviors CPE_1 and CPE_2, respectively. The sloping line is attributed to the solid-state Li diffusion into the active materials (Z_w). The experimental Nyquist plots are modeled based on the equivalent circuit. The fitted impedance parameters are listed in Table S1 (Supporting Information). The R_p (159.10 Ω) and R_{ct} (100.70 Ω) of SPs sum to 259.80 Ω, which is significantly lower than that of sulfur (494.25 Ω) with its corresponding R_p (66.15 Ω) and R_{ct} (428.10 Ω). This demonstrated that the incorporation of polyaniline can improve the electrical conductivity of the composite of SPs. After the introduction of GNRs in polyaniline, the sum of R_p (95.29 Ω) and R_{ct} (82.58 Ω) in SPGs is 177.87 Ω, which is significantly lower than 259.80 Ω in SPs. This demonstrates that the GNRs enhance the electrical conductivity of the SPGs, resulting in the improvement in the electrochemical performance.

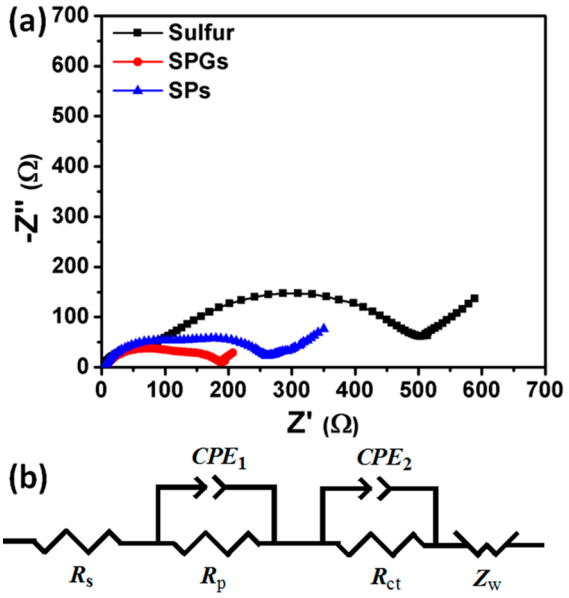

Figure 5. (a) Nyquist plots of sulfur, SPs, and SPGs. (b) Equivalent circuit that is used to fit experimental data.

4. CONCLUSIONS

In summary, we successfully designed and synthesized a hierarchical structure composite of sulfur−polyaniline−graphene nanoribbons. In this composite, GNRs greatly improved the mechanical properties of the whole system. PANI−GNRs provided a good platform for loading sulfur with improved electronic conductivity. Electrochemical experiments demonstrate that the SPGs exhibit good rate performance and high cycling stability as cathode materials, compared to pure elemental sulfur and sulfur−polyaniline, due to the synergic effect between the PANI, GNRs, and sulfur. The synthesis of the SPG composite has been shown to produce an effective component to improve the electrochemical stability of the electrode materials for LSBs.

■ ASSOCIATED CONTENT

Supporting Information

Additional SEM, XPS, XRD, and CV figures for sulfur, SPs and SPGs; table listing EIS simulation parameters of sulfur, SPs, and

SPGs. This material is available free of charge via the Internet at http://pubs.acs.org.

AUTHOR INFORMATION

Corresponding Author

*E-mail: tour@rice.edu. Tel.: (713) 348-6246. Fax: (713) 348-6250.

Notes

The authors declare no competing financial interest.

ACKNOWLEDGMENTS

The ONR MURI program (No. 00006766, N00014-09-1-1066), the AFOSR MURI program (FA9550-12-1-0035), the AFOSR (FA9550-09-1-0581), and the Chinese Scholarship Council provided funding.

REFERENCES

(1) Yang, Y.; Yu, G.; Cha, J. J.; Wu, H.; Vosgueritchian, M.; Yao, Y.; Bao, Z.; Cui, Y. Improving the Performance of Lithium-Sulfur Batteries by Conductive Polymer Coating. *ACS Nano* **2011**, *5*, 9187−9193.

(2) Tarascon, J. M.; Armand, M. Issues and Challenges Facing Rechargeable Lithium Batteries. *Nature* **2001**, *414*, 359−367.

(3) Arico, A. S.; Bruce, P.; Scrosati, B.; Tarascon, J. M.; Schalkwijk, W. V. Nanostructured Materials for Advanced Energy Conversion and Storage Devices. *Nat. Mater.* **2004**, *4*, 366−377.

(4) Whittingham, M. S. Lithium Batteries and Cathode Materials. *Chem. Rev.* **2004**, *104*, 427−4302.

(5) Zhou, G.; Yin, L. C.; Wang, D. W.; Li, L.; Pei, S.; Gentle, I. R.; Li, F.; Cheng, H. M. Fibrous Hybrid of Graphene and Sulfur Nanocrystals for High-Performance Lithium-Sulfur Batteries. *ACS Nano* **2013**, *7*, 5367−5375.

(6) Ji, X. L.; Lee, K. T.; Nazar, L. F. A Highly Ordered Nanostructured Carbon-Sulphur Cathode for Lithium-Sulphur Batteries. *Nat. Mater.* **2009**, *8*, 500−506.

(7) Ellis, B. L.; Lee, K. T.; Nazar, L. F. Positive Electrode Materials for Li-Ion and Li-Batteries. *Chem. Mater.* **2010**, *22*, 691−714.

(8) Rauh, R. D.; Abraham, K. M.; Pearson, G. F.; Surprenant, J. K.; Brummer, S. B. A Lithium/Dissolved Sulfur Battery with an Organic Electrolyte. *J. Electrochem. Soc.* **1979**, *126*, 523−527.

(9) Barchasz, C.; Molton, F.; Duboc, C.; Leprêtre, J. C.; Patoux, S.; Alloin, F. Lithium/Sulfur Cell Discharge Mechanism: An Original Approach for Intermediate Species Identification. *Anal. Chem.* **2012**, *84*, 3973−3980.

(10) Evers, S.; Nazar, L. F. New Approaches for High Energy Density Lithium-Sulfur Battery Cathodes. *Acc. Chem. Res.* **2012**, *46*, 1135−1143.

(11) Dean, J. A. *Lange's Handbook of Chemistry*, 3rd ed.; McGraw-Hill: New York, 1985; pp 3−5.

(12) Yang, Y.; Zheng, G.; Cui, Y. Nanostructured Sulfur Cathodes. *Chem. Soc. Rev.* **2013**, *42*, 3018−3032.

(13) Xiao, L.; Cao, Y.; Xiao, J.; Schwenzer, B.; Engelhard, M. H.; Saraf, L. V.; Nie, Z.; Exarhos, G. J.; Liu, J. A Soft Approach to Encapsulate Sulfur: Polyaniline Nanotubes for Lithium-Sulfur Batteries with Long Cycle Life. *Adv. Mater.* **2012**, *24*, 1176−1181.

(14) Wang, H.; Yang, Y.; Liang, Y.; Robinson, J. T.; Li, Y.; Jackson, A.; Cui, Y.; Dai, H. Graphene-Wrapped Sulfur Particles as a Rechargeable Lithium-Sulfur Battery Cathode Material with High Capacity and Cycling Stability. *Nano Lett.* **2011**, *11*, 2644−2647.

(15) Evers, S.; Nazar, L. F. Graphene-Enveloped Sulfur in a One Pot Reaction: A Cathode with Good Coulombic Efficiency and High Practical Sulfur Content. *Chem. Commun.* **2012**, *48*, 1233−1235.

(16) Guo, J.; Xu, Y.; Wang, C. Sulfur-Impregnated Disordered Carbon Nanotubes Cathode for Lithium-Sulfur Batteries. *Nano Lett.* **2011**, *11*, 4288−4294.

(17) Wu, F.; Chen, J.; Chen, R.; Wu, S.; Li, L.; Chen, S.; Zhao, T. Sulfur/Polythiophene with a Core/Shell Structure: Synthesis and Electrochemical Properties of the Cathode for Rechargeable Lithium Batteries. *J. Phys. Chem. C* **2011**, *115*, 6057−6063.

(18) Yu, X.; Xie, J.; Li, Y.; Huang, H.; Lai, C.; Wang, K. Stable-cycle and High-capacity Conductive Sulfur-Containing Cathode Materials for Rechargeable Lithium Batteries. *J. Power Sources* **2005**, *146*, 335−339.

(19) Li, X.; Cao, Y.; Qi, W.; Saraf, L. V.; Xiao, J.; Nie, Z.; Mietek, J.; Zhang, J. G.; Schwenzer, B.; Liu, J. Optimization of Mesoporous Carbon Structures for Lithium-sulfur Battery applications. *J. Mater. Chem.* **2011**, *21*, 16603−16610.

(20) Zheng, G.; Yang, Y.; Cha, J. J.; Hong, S. S.; Cui, Y. Hollow Carbon Nanofiber-Encapsulated Sulfur Cathodes for High Specific Capacity Rechargeable Lithium Batteries. *Nano Lett.* **2011**, *11*, 4462−4467.

(21) Zheng, G.; Zhang, Q.; Cha, J. J.; Yang, Y.; Li, W.; Seh, Z. W.; Cui, Y. Amphiphilic Surface Modification of Hollow Carbon Nanofibers for Improved Cycle Life of Lithium Sulfur Batteries. *Nano Lett.* **2013**, *13*, 1265−1270.

(22) Li, D.; Han, F.; Wang, S.; Cheng, F.; Sun, Q.; Li, W. C. High Sulfur Loading Cathodes Fabricated Using Peapodlike, Large Pore Volume Mesoporous Carbon for Lithium-Sulfur Battery. *ACS Appl. Mater. Interfaces* **2013**, *5*, 2208−2213.

(23) Zhang, S. S. Liquid Electrolyte Lithium/sulfur Battery: Fundamental Chemistry, Problems, and Solutions. *J. Power Sources* **2013**, *231*, 153−162.

(24) Zhang, S. S. Role of $LiNO_3$ in Rechargeable Lithium/sulfur Battery. *Electrochim. Acta* **2012**, *70*, 344−348.

(25) Barchasz, C.; Leprêtre, J. C.; Alloin, F.; Patoux, S. New Insights into the Limiting Parameters of the Li/S Rechargeable Cell. *J. Power Sources* **2012**, *199*, 322−330.

(26) Nimon, Y. S.; Chu M. Y.; Visco, S. J. U.S. Patent 6,632,573, 2003.

(27) Lee, Y. M.; Choi, N. S.; Park, J. H.; Park, J. K. Electrochemical Performance of Lithium/sulfur Batteries with Protected Li Anodes. *J. Power Sources* **2003**, *119*, 964−972.

(28) Li, K.; Wang, B.; Su, D.; Park, J.; Ahn, H.; Wang, G. Enhanced Electrochemical Performance of Lithium Sulfur Battery Through a Solution-Based Processing Technique. *J. Power Sources* **2012**, *202*, 389−393.

(29) Wu, F.; Chen, J. Z.; Li, L.; Zhao, T.; Chen, R. J. Improvement of Rate and Cycle Performance by Rapid Polyaniline Coating of a MWCNT/Sulfur Cathode. *J. Phys. Chem. C* **2011**, *115*, 24411−24417.

(30) Jayaprakash, N.; Shen, J.; Moganty, S. S.; Corona, A.; Archer, L. A. Confining Sulfur in Double-Shelled Hollow Carbon Spheres for Lithium-Sulfur Batteries. *Angew. Chem., Int. Ed.* **2011**, *50*, 5904−5908.

(31) Zhang, C.; Wu, H. B.; Yuan, C.; Guo, Z.; Lou, X. W. Confining Sulfur in Double-Shelled Hollow Carbon Spheres for Lithium-Sulfur Batteries. *Angew. Chem., Int. Ed.* **2012**, *51*, 9592−9595.

(32) Seh, Z. W.; Li, W. Y.; Cha, J. J.; Zheng, G. Y.; Yang, Y.; Mcdowell, M. T.; Hsu, P. C.; Cui, Y. Sulphur−TiO_2 Yolk−shell Nanoarchitecture with Internal Void Space for Long-cycle Lithium-sulphur Batteries. *Nat. Commun.* **2012**, *4*, 1331−1336.

(33) Evers, S.; Yim, T.; Nazar, L. F. Understanding the Nature of Absorption/Adsorption in Nanoporous Polysulfide Sorbents for the Li-S Battery. *J. Phys. Chem. C* **2012**, *116*, 19653−19658.

(34) Li, G. C.; Li, G. R.; Ye, S. H.; Gao, X. P. A Polyaniline-Coated Sulfur/Carbon Composite with an Enhanced High-Rate Capability as a Cathode Material for Lithium/Sulfur Batteries. *Adv. Energy. Mater.* **2012**, *2*, 1238−1245.

(35) Hager, M. D.; Greil, P.; Leyens, C.; Van der Zwaag, S.; Schubert, U. S. Self-Healing Materials. *Adv. Mater.* **2010**, *22*, 5424−5430.

(36) Li, L.; Raji, A. R. O.; Fei, H.; Yang, Y.; Samuel, E. L. G.; Tour, J. M. Nanocomposite of Polyaniline Nanorods Grown on Graphene Nanoribbons for Highly Capacitive Pseudocapacitors. *ACS Appl. Mater. Interfaces* **2013**, *5*, 6622−6627.

(37) Genorio, B.; Lu, W.; Dimiev, A. M.; Zhu, Y.; Raji, A.R. O.; Novosel, B.; Alemany, L. B.; Tour, J. M. *In Situ* Intercalation Replacement and Selective Functionalization of Graphene Nanoribbon Stacks. *ACS Nano* **2012**, *6*, 4231−4240.

(38) Cao, Y.; Li, X.; Aksay, I. A.; Lemmon, J.; Nie, Z.; Yang, Z.; Liu, J. Sandwich-type Functionalized Graphene Sheet-sulfur Nanocomposite for Rechargeable Lithium Batteries. *Phys. Chem. Chem. Phys.* **2011**, *13*, 7660−7665.
(39) Li, N.; Zheng, M.; Lu, H.; Hu, Z.; Shen, C.; Chang, X.; Ji, G.; Cao, J.; Shi, Y. High-rate Lithium-sulfur Batteries Promoted by Reduced Graphene Oxide Coating. *Chem. Commun.* **2012**, *48*, 4106−4108.
(40) Semmelhack, H. C.; Höhne, R.; Esquinazi, P.; Wagner, G.; Rahm, A.; Hallmeier, K. H.; Spemann, D.; Schindler, K. Growth of Highly Oriented Graphite Films at Room Temperature by Pulsed Laser Deposition Using Carbon-sulfur Targets. *Carbon* **2006**, *44*, 3064−3072.
(41) Ji, L.; Rao, M.; Zheng, H.; Zhang, L.; Li, Y.; Duan, W.; Guo, J.; Cairns, E. J.; Zhang, Y. Graphene Oxide as a Sulfur Immobilizer in High Performance Lithium/Sulfur Cells. *J. Am. Chem. Soc.* **2011**, *133*, 18522−18525.
(42) Zu, C.; Su, Y. S.; Fu, Y.; Manthiram, A. Improved lithium−sulfur cells with a treated carbon paper interlayer. *Phys. Chem. Chem. Phys.* **2013**, *15*, 2291−2297.